



1 **Impacts of an aerosol layer on a mid-latitude continental system of cumulus clouds:**
2 **how do these impacts depend on the vertical location of the aerosol layer?**

3

4 Seoung Soo Lee^{1,2}, Junshik Um^{3,4}, Won Jun Choi⁵, Kyung-Ja Ha^{2,4,6}, Chang Hoon Jung⁷,
5 Jianping Guo⁸, Youtong Zheng⁹

6

7 ¹Earth System Science Interdisciplinary Center, University of Maryland, Maryland, USA

8 ²Research Center for Climate Sciences, Pusan National University, Busan, Republic of
9 Korea

10 ³Department of Atmospheric Sciences, Pusan National University, Busan, Republic of
11 Korea

12 ⁴BK21 School of Earth and Environmental Systems, Pusan National University, Busan,
13 Republic of Korea

14 ⁵National Institute of Environmental Research, Incheon, Republic of Korea

15 ⁶Center for Climate Physics, Institute for Basic Science, Busan, Republic of Korea

16 ⁷Department of Health Management, Kyungin Women's University, Incheon, Republic of
17 Korea

18 ⁸State Key Laboratory of Severe Weather, Chinese Academy of Meteorological Sciences,
19 Beijing, China

20 ⁹The Program in Atmospheric and Oceanic Sciences, Princeton University, Princeton,
21 New Jersey, USA

22

23

24



25 Corresponding authors: Seoung Soo Lee and Junshik Um
26 E-mail: cumulss@gmail.com, slee1247@umd.edu, jjunum@pusan.ac.kr
27
28
29
30
31
32
33
34
35
36
37
38
39
40
41
42
43
44
45
46
47
48
49
50
51



52 **Abstract**

53

54 Using the large-eddy simulation framework, effects of an aerosol layer on warm cumulus
55 clouds in the Korean Peninsula when the layer is above or around the cloud tops in the
56 upper atmosphere are examined. Also, these effects are compared to effects of an aerosol
57 layer when it is around or below the cloud bases in the low atmosphere. Simulations show
58 that when the aerosol layer is in the low atmosphere, aerosols absorb solar radiation and
59 radiatively heat up air enough to induce greater instability, stronger updrafts and more
60 cloud mass than when the layer is in the upper atmosphere. As aerosol concentrations in
61 the layer decrease, the aerosol radiative heating gets weaker to lead to less instability,
62 weaker updrafts and less cloud mass when the layer is in the low atmosphere. This in turn
63 makes differences in cloud mass, which are between a situation when the layer is in the
64 low atmosphere and that when the layer is in the upper atmosphere, smaller. It is found that
65 the transportation of aerosols by updrafts reduces aerosol concentrations in the aerosol
66 layer, which is in the low atmosphere, and in turn reduces the aerosol radiative heating,
67 updraft intensity and cloud mass. It is also found that the presence of aerosol impacts on
68 radiation suppresses updrafts and reduces clouds. Aerosols affect not only radiation but
69 also aerosol activation. In the absence of aerosol impacts on radiation, aerosol impacts on
70 the droplet nucleation increases cloud mass when the layer is in the low atmosphere as
71 compared to a situation when the layer is in the upper atmosphere. As aerosol impacts on
72 radiation team up with those on the droplet nucleation, differences in cloud mass, which
73 are between a situation when the layer in the low atmosphere and that when the layer is in
74 the upper atmosphere, get larger. This is as compared to a situation when there is no aerosol
75 impacts on radiation and only aerosol impacts on the droplet nucleation.

76

77

78

79

80

81

82



83 **1. Introduction**

84

85 Warm cumulus clouds play an important role in global hydrologic and energy circulations
86 (Warren et al., 1986; Stephens and Greenwald, 1991; Hartmann et al., 1992; Hahn and
87 Warren, 2007; Wood, 2012). With industrialization, there have been significant increases
88 in concentrations of aerosols acting as cloud condensation nuclei (CCN) and these
89 increases are known to decrease droplet size (Twomey, 1974, 1977). Increases in
90 concentrations of aerosols acting as radiation absorbers are also known to enhance the
91 radiative heating of air by aerosols. These aerosol-induced changes in droplet size and
92 radiative heating affect updrafts, cloud mass, cloud albedo and precipitation (Albrecht,
93 1989; Hansen et al., 1997). Global hydrologic and energy circulations are eventually
94 affected by these aerosol effects. However, these effects, which are particularly on warm
95 cumulus clouds, are highly uncertain and thus act to cause the highest uncertainty in the
96 prediction of future climate (Ramaswamy et al., 2001; Forster et al., 2007).

97 In recent years, people start to take interest in effects of aerosol layers above or around
98 the tops of clouds on clouds (e.g., de Graaf et al., 2014; Xu et al., 2017). This interest is
99 motivated by aerosol layers that are originated from biomass burning sites in the southern
100 Africa. These layers are lifted and transported to the southeast Atlantic (SEA) region and
101 located above or around the top of a large deck of warm cumulus and stratocumulus clouds
102 that play an important role in global hydrologic and energy circulations. Note that aerosols
103 in the transported aerosol layers contain organic carbon (OC) and black carbon (BC) that
104 act as radiation absorbers as well as cloud condensation nuclei (CCN). When these aerosols
105 act as radiation absorbers, they absorb solar radiation and heat up the atmosphere to change
106 atmospheric stability. This in turn affects the cumulus clouds, the hydrologic and energy
107 circulations, and climate. When these aerosols act as CCN, they have an impact on aerosol
108 activation, subsequent microphysical and precipitation processes in the cumulus clouds,
109 those circulations and climate. Reflecting the interest and an associated potential
110 importance of aerosol layers above or around cloud tops in the circulations and climate, to
111 better understand roles of aerosol layers above or around cloud tops in cloud development
112 and its impacts on climate, there were international field campaigns in the SEA such as the
113 NASA ObseRvations of Aerosols above CLouds and their intEractionS (ORACLES;



114 <https://espo.nasa.gov/oracles/content/ORACLES>), the UK Clouds and Aerosol Radiative
115 Impacts and Forcing (CLARIFY; Redemann et al., 2021) and the French Aerosol,
116 Radiation and Clouds in southern Africa (AEROCLO-sA; Formenti et al., 2019)
117 campaigns.

118 It is well-known that the relative vertical location of an aerosol layer and a cloud deck
119 can affect cloud properties (e.g., updrafts, cloud mass and albedo) that responds to aerosol
120 absorption, subsequent changes in atmospheric stability, aerosol activation and subsequent
121 changes in microphysics and precipitation (Haywood and Shine, 1997; Johnson et al., 2004;
122 McFarquhar and Wang, 2006). However, despite above-mentioned field campaigns,
123 previous studies on aerosol-cloud interactions have focused mainly on effects of aerosols
124 around or below cloud bottoms on clouds. Effects of aerosols above or around cloud tops
125 on clouds have not been examined as much. This contributes to the low-level understanding
126 of effects of the relative location of an aerosol layer and a cloud deck on the cloud deck.
127 Improving this understanding, which is about going beyond the traditional approach that
128 focuses on around- or below-cloud-bottom aerosol layers, is likely to contribute to the more
129 comprehensive understanding of aerosol-cloud-radiation interactions and thus more
130 general parameterizations of those interactions for climate models. Hence, this study aims
131 to enhance our understanding of effects of the relative location of an aerosol layer and a
132 cloud deck on the cloud deck. This aim is pursued by investigating aerosol-cloud-radiation
133 interactions in a typical situation where an aerosol layer is around or below the bottom of
134 a system of warm cumulus clouds. Then, to fulfill the aim, these interactions in the typical
135 situation are compared to a situation where an aerosol layer is around or above the top of
136 the system. In this study, the investigation is performed by using simulations adopting the
137 large-eddy simulation (LES) framework and an idealized setup, which is based on
138 observation, for the aerosol layer.

139

140 **2. Case, model and simulations**

141

142 **2.1 LES model**

143



144 The Advanced Research Weather Research and Forecasting (ARW) model is for LES
145 simulations in this study. The ARW model is a compressible model with a nonhydrostatic
146 status. A 5th-order monotonic advection scheme is used to advect microphysical variables
147 (Wang et al., 2009). The ARW adopts a bin scheme to parameterize microphysics. The
148 Hebrew University Cloud Model (HUCM) detailed in Khain et al. (2011) is the bin scheme.
149 A set of kinetic equations is solved by the bin scheme to represent size distribution
150 functions for each class of hydrometeors and aerosols acting as cloud condensation nuclei
151 (CCN). The hydrometeor classes are water drops, ice crystals (plate, columnar and branch
152 types), snow aggregates, graupel and hail. There are 33 bins for each size distribution in a
153 way that the mass of a particle m_j in the j bin is to be $m_j = 2m_{j-1}$.

154 Aerosol sinks and sources control the evolution of aerosol size distribution. These
155 sinks and sources include advection and aerosol activation (Fan et al., 2009). Activated
156 particles are emptied in the corresponding bins of the aerosol spectra. Aerosol mass
157 included in hydrometeors, after activation, is moved to different classes and sizes of
158 hydrometeors through collision-coalescence and removed from the atmosphere once
159 hydrometeors that contain aerosols reach the surface.

160 The Rapid Radiation Transfer Model (RRTM; Mlawer et al., 1997) has been coupled
161 to the bin microphysics scheme described above. Aerosols before their activation can affect
162 radiation by changing the reflection, scattering, and absorption of radiation. This radiative
163 effect of aerosol is represented following Feingold et al. (2005). The internal aerosol
164 mixture and the ARW relative humidity are used to calculate the hygroscopic growth of
165 the aerosol particles as well as their optical properties, represented by extinction, single
166 scattering albedo, and asymmetry factor. Aerosol uptake of water vapor is considered over
167 the range of relative humidity in the domain. In practice, hygroscopic growth and optical
168 property calculations are performed offline prior to simulation and stored in lookup tables.
169 Calculations are done for the prescribed aerosol size distribution and composition, and unit
170 concentration. During model runtime, grid-point number concentration and relative
171 humidity determine the look-up table entries that specify the grid-point aerosol optical
172 properties. The effective sizes of hydrometeors are calculated in an adopted microphysics
173 scheme and the calculated sizes are transferred to the RRTM to consider effects of the
174 effective sizes on radiation.



175 The presence of the aerosol perturbs the radiative fluxes reaching the surface, and its
176 subsequent partitioning into sensible and latent heat fluxes (i.e., the Bowen ratio). This is
177 accounted for with the interactive Noah land surface model (Chen and Dudhia, 2001).

178

179 **2.2 Case and simulations**

180

181 **2.2.1 Case and standard simulations**

182

183 There is an observed system of warm cumulus clouds in a domain in the Korean Peninsula,
184 as marked in Figure 1, for a period between 10:00 and 18:00 LST on April 13th, 2015. This
185 system is simulated to fulfill the goal of this study. For a three-dimensional simulation (i.e.,
186 the control run) of the system in the domain over the period, a 50-m resolution is used for
187 the horizontal domain. The length of the domain in the east-west (north-south) direction is
188 20 (20) km. In the vertical domain, the resolution coarsens with height. The resolution in
189 the vertical domain is 20 m just above the surface and 100 m at the model top that is at ~
190 4.5 km in altitude. Initial and boundary conditions of potential temperature, specific
191 humidity, and wind for the simulation are provided by reanalysis data. These data are
192 produced by the Met Office Unified Model (Brown et al., 2012) every 6 hours on a 0.11°
193 $\times 0.11^\circ$ grid. These data represent the synoptic-scale environment. Figure 2 depicts the
194 vertical distributions of potential temperature and water-vapor mixing ratio at 09:00 LST
195 on April 15th, 2015 in radiosonde sounding that is obtained near the domain. This vertical
196 distribution represents initial environmental conditions for the development of the clouds
197 in the control run. The conditional instability is present in the vertical profiles and this
198 favors the development of warm cumulus clouds. An open lateral boundary condition is
199 employed for the control run.

200 There is a site of the aerosol robotic network (AERONET; Holben et al., 2001) in the
201 domain. At 10:00 LST when clouds in the domain start to develop, there is an aerosol layer
202 advected from the East Asia and this layer causes aerosol pollution in the domain. This
203 advection is monitored by aerosol-measuring stations in the Yellow sea as described in Lee
204 et al. (2021). According to the AERONET measurement, which is 1 hour before the
205 observed cumulus clouds start to form, aerosol particles in the layer, on average, are an



206 internal mixture of 70 % ammonium sulfate, 22 % organic compound and 8% black carbon.
207 Aerosol chemical composition in this study is assumed to be represented by this mixture
208 in the whole domain during the whole simulation period. Based on the AERONET
209 observation, the size distribution of background aerosols acting as CCN is assumed to
210 follow a bi-modal log-normal distribution. Modal radius of this distribution is 0.11 and 1.2
211 μm and standard deviation of this distribution is 1.71 and 1.92, while the partition of
212 aerosol number, which is normalized by the total aerosol number of the size distribution,
213 is 0.999 and 0.001 for accumulation and coarse modes, respectively. It is assumed that the
214 size distribution of background aerosols acting as CCN in all parts of the domain during
215 the whole simulation period is assumed to follow the bi-modal size distribution. The
216 average aerosol concentration in the layer over the domain at 10:00 LST is $\sim 15000\text{ cm}^{-3}$.
217 This average concentration is applied to all grid points in the layer at the first time step of
218 the control run. This aerosol layer is idealized to be located around and below cloud bases
219 between the surface and 1.0 km as shown in Figure 3a. Cloud bases are located around 1
220 km. Above the layer, aerosol concentration is assumed to be 150 cm^{-3} .

221 This study aims to understand differences in aerosol effects on warm cumulus clouds
222 between the situation where an aerosol layer is above and around the cloud tops and that
223 where the aerosol layer is around and below the cloud bases. To fulfill this goal, we repeat
224 the control run by an idealized setup where the aerosol layer is moved upward to altitudes
225 between 2.5 and 3.5 km as shown in Figure 3b. Altitudes between 2.5 and 3.5 km are places
226 where cloud tops are located frequently. Note that the simulated maximum cloud-top height
227 is 3.3 km. This repeated run is referred to as the aro-above-cld run. As shown in Figures
228 3a and 3b, aerosol concentrations in the aerosol layer are 15000 cm^{-3} in both of the runs.
229 Outside the main aerosol layer, aerosol concentration is set at 150 cm^{-3} in both of the runs
230 (Figures 3a and 3b). Here, we see that the depth of the main aerosol layer and aerosol
231 concentrations in the main layer are identical between the runs.

232 It is well-known that aerosol-cloud-radiation interactions are strongly dependent on
233 aerosol concentrations (Tao et al., 2012). We want to test how results in the control and
234 aro-above-cld runs are sensitive to aerosol concentrations in the main aerosol layer. For
235 the test, the control and aro-above-cld runs are repeated with 10 times lower aerosol
236 concentrations in the main aerosol layer but with no changes in aerosol concentrations in



237 the domain outside the main aerosol layer. In these repeated runs, the aerosol concentration
238 in the main aerosol layer at the first time step is 1500 cm^{-3} . Henceforth, the repeated control
239 and aro-above-cld runs are referred to as the control-1500 and aro-above-cld-1500 runs.

240

241 **2.2.2 Additional simulations**

242

243 Clouds affect aerosols by cloud processes such as nucleation of droplets and aerosol
244 transportation (or advection) by cloud-induced wind. Updrafts and downdrafts comprise
245 cloud-induced wind and transport aerosols upward and downward, respectively. Here, we
246 are interested in impacts of clouds on aerosols and how these impacts in turn affect aerosol
247 effects on clouds. To examine these aspects of aerosol-cloud interactions, the above-
248 mentioned four standard simulations (e.g., the control, aro-above-cld, control-1500 and
249 aro-above-cld-1500 runs) are repeated by preventing aerosol evolution with time at each
250 grid point. In other words, in these repeated runs, aerosol concentrations at each grid point,
251 which are set at the first time step, do not vary with time or are not affected by cloud
252 processes such as nucleation and advection. These repeated runs are referred to as the
253 control-novary, aro-above-cld-novary, control-1500-novary, and aro-above-cld-1500-
254 novary runs. By comparing the standard simulations to these repeated ones, roles of cloud
255 impacts on aerosols in aerosol-layer impacts on clouds are identified.

256 In this study, we aim to better understand roles of the interception (e.g., reflection,
257 scattering and absorption) of radiation by aerosols, which results in phenomena such as
258 radiative heating of air by aerosols. These roles are referred to as aerosol radiative effects.
259 To better understand aerosol radiative effects, the above four standard simulations are
260 repeated again by turning off aerosol radiative effects. These repeated runs are the control-
261 norad, aro-above-cld-norad, control-1500-norad, aro-above-cld-1500-norad runs. The
262 summary of simulations in this study is given in Table 1.

263

264 **3. Results**

265

266 **3.1 The control and aro-above-cld runs**

267



268 Figure 4 shows the time- and area-averaged vertical distributions of cloud-liquid mass
269 density that represents cloud mass for the standard simulations. In Figure 4, the cloud layer
270 is between 1.0 and 3.3 km in the control run and between 0.8 and 2.6 km in the aro-above-
271 cld run. The time- and domain-averaged cloud-liquid mass density is 0.7 and 1.3×10^{-3} g
272 m^{-3} in the control run and in the aro-above-cld run, respectively. Hence, we see that clouds
273 are thicker with their higher tops and have greater mass in the control run than in the aro-
274 above-cld run. This is despite the fact that aerosol concentrations in the main aerosol layer
275 in the control run are identical to those in the aro-above-cld run.

276 Figure 5a shows the time series of the domain-averaged liquid-water path, which is
277 the vertical integral of cloud-liquid mass density and thus, represents cloud mass, for the
278 standard simulations. During the initial stage of the cloud development between 12:50 and
279 13:50 LST, the average cloud mass is slightly higher in the control run than in the aro-
280 above-cld run. Also, the average non-zero cloud mass starts to appear earlier in the control
281 run than in the aro-above-cld run. Over the period between 13:50 and 14:10 LST, there is
282 a jump (or rapid increase or surge) in the average cloud mass in the control run but not in
283 the aro-above-cld run. During this period with the jump, at some specific time points, the
284 average mass is \sim one order of magnitude higher in the control run than in the aro-above-
285 cld run. Of interest is that just after the jump and at 14:10 LST, the average mass in the
286 control run starts to decrease and at 14:40 LST, becomes lower than that in the aro-above-
287 cld run. Hence, the greater time- and domain-averaged cloud mass in the control run is
288 mainly attributed to the jump in cloud mass. As seen in Figures 5b and 5c that show the
289 time series of the domain-averaged updraft speed and condensation rates, respectively, the
290 average updraft mass fluxes and associated condensation rates in the control run are also
291 slightly higher in the control run than in the aro-above-cld run for the period between 12:50
292 and 13:50 LST. The average updraft speed and associated condensation rates in the control
293 run jump during the period between \sim 13:50 and \sim 14:10 LST, hence, these speed and rates
294 are much higher in the control run than in the aro-above-cld run during the period between
295 \sim 13:50 and \sim 14:10 LST (Figures 5b and 5c). After the jump, the speed and rates decrease
296 rapidly and become lower in the control run than in the aro-above-cld run (Figures 5b and
297 5c). Taking into account the fact that condensation is the only source of cloud mass and
298 the updraft speed strongly control the amount of condensation, the updraft speed,



299 condensation rate and cloud mass in each of the runs and differences in those variables
300 between the runs are similar in terms of their temporal evolution.

301 Figure 5d shows the time series of the domain-averaged convective available potential
302 energy (CAPE) for the control and aro-above-cld runs. Considering that updrafts grow by
303 consuming buoyancy energy, updraft intensity is proportional to CAPE that is the integral
304 of the buoyancy energy in the vertical domain. Hence, the evolution of CAPE in each of
305 the runs is similar to that of the updraft speed, associated condensation rates and cloud
306 mass. Accordingly, the evolution of differences in CAPE between the runs is similar to that
307 of those differences in the updraft speed, associated condensation rates and cloud mass.
308 This similarity includes the jump not only in CAPE but also in those speed, rates and mass
309 during the period between 13:50 and 14:10 LST in the control run. (052022)

310 In Figures 5, the peaks (or the maximum values) of the domain-averaged CAPE,
311 updrafts, condensation rates and cloud mass in the control run occur around 14:10 LST and
312 this occurrence is earlier than that which occurs around 14:50 LST in the aro-above-cld
313 run. This means that the cloud system in the control run reaches its mature stage earlier
314 than that in the aro-above-cld run. After the peak around 14:10 LST, the system enters its
315 dissipating stage in the control run, while around 14:10 LST in the aro-above-cld run, the
316 system still evolves to enter the mature stage and it enters its dissipating stage after 14:50
317 LST. Hence, the cloud system in the control run matures and demises faster as compared
318 to that in the aro-above-cld run. Stated differently, the cloud system in the control run has
319 a shorter life cycle than that in the aro-above-cld run.

320 To find mechanisms controlling the jump in CAPE which acts as a main cause of the
321 greater cloud mass in the control run, the analysis of the results is done for an initial period
322 between 10:00 LST when the simulation starts and 13:50 LST which is immediately before
323 the jump starts to occur. The thermodynamic condition for the CAPE jump is established
324 during this initial period. The average net shortwave fluxes at the surface are shown in
325 Table 2 for the initial period in the control and aro-above-cld runs. Table 2 shows that
326 during the initial period in the control run, there is a smaller amount of shortwave radiation
327 that are incident on the surface in the control run than in the aro-above-cld run. The aerosol
328 layer intercepts solar radiation and reduces solar radiation which reaches the surface. In
329 spite of the fact that the depth of the main aerosol layer and aerosol concentrations in the



330 layer are identical between the runs, results here indicate that the aerosol layer in the low
331 atmosphere is more efficient in the interception of solar radiation than that in the upper
332 atmosphere. Due to the less solar radiation reaching the surface, the time- and area-
333 averaged net surface heat fluxes, which are the sum of the surface sensible and latent-heat
334 fluxes, become lower in the control run than in the aro-above-cld run during the initial
335 period (Table 2). Hence, the surface fluxes favor more instability or higher CAPE and
336 associated more intense subsequent updrafts and cloud mass in the aro-above-cld run than
337 in the control run.

338 The vertical distributions of the time- and domain-averaged radiative heating rates are
339 obtained for the initial period for each of the control and aro-above-cld runs. For the initial
340 period, the average radiative heating rate is much higher in the control run than in the aro-
341 above-cld run particularly at altitudes between 0.0 and ~ 1.0 km where cloud bases are
342 located (Figure 6a). This is associated with the fact that the main aerosol layer is located at
343 altitudes between 0.0 and 1.0 km in the control run. This more radiative heating in the low
344 atmosphere favors subsequent higher CAPE, which involves its jump in the control run, in
345 the control run than in the aro-above-cld run after the initial period. The average radiative
346 heating rate is higher in the aro-above-cld run than in the control run at altitudes between
347 ~ 2.5 and 3.5 km. This is associated with the fact that the main aerosol layer is located at
348 altitudes between 2.5 and 3.5 km in the aro-above-cld run. However, this higher radiative
349 heating rate is in the upper part of the domain and tends to stabilize the atmosphere more
350 in the aro-above-cld run than in the control run. Thus, the higher radiative heating rate in
351 the aro-above-cld run contributes to lower CAPE, less intense updrafts and lower cloud
352 mass in the aro-above-cld run especially for the period when the jumps occur in the control
353 run.

354 Effects of greater radiative heating in the low atmosphere on CAPE outweigh those
355 effects of solar radiation which are incident on the surface and the associated surface heat
356 fluxes during the initial stage in the control run. This leads to more intense clouds with
357 more cloud mass for the rest of periods, in turn leading to the more time- and domain-
358 averaged cloud mass in the control run than in the aro-above-cld run.

359

360 **3.2 Comparisons between simulations with different aerosol concentrations**



361

362 With the lower concentration of aerosols in the main layer, there are much more solar
363 radiation reaching the surface and resultant higher surface fluxes in the control-1500 run
364 than in the control run and in the aro-above-cld-1500 run than in the aro-above-cld run
365 (Table 2). This makes CAPE higher in the control-1500 run than in the control run over
366 most of the simulation period except for the period between 13:50 and 14:20 LST during
367 which the jump in CAPE in the control run exists, and in the aro-above-cld-1500 run than
368 in the aro-above-cld run throughout the simulation period (Figure 5d). Then, there are
369 stronger updrafts and greater condensation rate and cloud-liquid mass density developing
370 in the control-1500 run than in the control run over most of the simulation period, which
371 are except for the period between 13:50 and 14:20 LST during which the jump in updrafts
372 and cloud-liquid mass in the control run exists, and in the aro-above-cld-1500 run than in
373 the aro-above-cld run throughout the simulation period (Figures 5a, 5b and 5c). This leads
374 to the greater time- and domain-averaged cloud-liquid mass density in the control-1500 run
375 than in the control run and in the aro-above-cld-1500 run than in the aro-above-cld run
376 (Figure 4). Regarding the control and control-1500 runs, this is despite the fact that aerosol
377 radiative heating in the main aerosol layer in the low atmosphere is higher due to higher
378 aerosol concentrations there in the control run than in the control-1500 run (Figure 6). In
379 Figure 4, it is seen that the time- and domain-averaged cloud-liquid mass in the aro-above-
380 cld-1500 run is higher than in the control run. This is due to more solar radiation reaching
381 the surface in the aro-above-cld-1500 run than in the control run and despite the fact that
382 aerosol concentrations and thus aerosol radiative heating in the low atmosphere is much
383 higher in the control run than in the aro-above-cld-1500 run (Table 2 and Figure 6). In
384 Figure 4, it is also seen that the time- and domain-averaged cloud-liquid mass in the
385 control-1500 run is higher than in the aro-above-cld run. This is due to higher aerosol
386 concentrations and more aerosol radiative heating in the low atmosphere (in the upper
387 atmosphere) in the control-1500 run (aro-above-cld run) than in the aro-above-cld run
388 (control-1500 run).

389 Similar to the situation between the control and aro-above-cld runs, there is less solar
390 radiation reaching the surface in the control-1500 run than in the aro-above-cld-1500 run
391 (Table 2). In association with this, there is the less surface heat fluxes in the control-1500



392 run than in the aro-above-cld-1500 run. This favors higher CAPE and more invigoration of
393 updrafts and associated convection in the aro-above-cld-1500 run than in the control-1500
394 run. However, overall, CAPE is higher in the control-1500 run than in the aro-above-cld-
395 1500 run (Figure 5d). This is because similar to the situation between the control and aro-
396 above-cld runs, more aerosols are in the low atmosphere in the control-1500 run than in
397 the aro-above-cld-1500 run. These more aerosols heat up the low atmosphere more and
398 increase the instability there more (Figure 6c). This induces increases in CAPE, which
399 compensates for decreases in CAPE due to the smaller amount of solar radiation reaching
400 the surface in the control-1500 run, and leads to overall higher CAPE in the control-1500
401 run than in the aro-above-cld-1500 run.

402 Associated with higher CAPE, there is greater cloud-liquid mass density in the control-
403 1500 run than in the aro-above-cld-1500 run, which is similar to the situation between the
404 control and aro-above-cld runs. However, differences in the mass density between these
405 repeated runs are smaller than those between the control and aro-above-cld runs (Figure 4).
406 As seen in Figure 5a which shows the time series of the domain-averaged cloud-liquid
407 mass density, the control-1500 run does not show a jump in the mass density unlike the
408 situation in the control run. This contributes to smaller differences in cloud-liquid mass
409 density between the control-1500 and aro-above-cld-1500 runs than between the control
410 and aro-above-cld runs. The CAPE evolution of the control-1500 and aro-above-cld-1500
411 runs show that there is no jump in CAPE and thus updrafts in the control-1500 run (Figure
412 5d). This mainly contributes to smaller differences in CAPE and updrafts, which in turn
413 contributes to smaller differences in cloud mass between the control-1500 and aro-above-
414 cld-1500 runs than between the control and aro-above-cld runs.

415 In addition, remember that the cloud system in the control run has a shorter life cycle
416 than in the aro-above-cld run. However, as seen in Figure 5, the cloud system the control-
417 1500 run has a similar life cycle to that in the aro-above-cld-1500 run. In the control run,
418 the instability or CAPE accumulates or increases rapidly to reach its peak, which forms the
419 jump, for a period between 13:50 and 14:10 LST, while in the control-1500 run, CAPE
420 increases gradually to reach its peak from ~12:00 LST to ~14:30 LST (Figure 5d). For a
421 period between ~14:10 and ~14:50 LST, CAPE reduces rapidly down back to the CAPE
422 value around ~13:00 LST in the control run, while CAPE decreases gradually and never



423 drops back to CAPE value at ~12:00 LST until the end of the simulation period in the
424 control-1500 run. This leads to the shorter life cycle or lifetime of the system not only in
425 the control run than in the aro-above-cld run but also in the control run than in the control-
426 1500 run. Here, we see that as aerosol concentration increases in the main aerosol layer in
427 the low atmosphere, the time scale of the accumulation and consumption of the instability
428 or convective energy gets shorter, leading to the shorter lifetime of the cloud system. When
429 aerosol concentration in the main aerosol layer in the low atmosphere is relatively low as
430 in the control-1500 run, the relatively long lifetime of the cloud system in the control-1500
431 run is similar to the lifetime in the aro-above-cld-1500 run. However, when aerosol
432 concentration in the main aerosol layer in the low atmosphere is relatively high as in the
433 control run, the relatively short lifetime of the cloud system in the control run is shorter
434 than the lifetime in the aro-above-cld run.

435 Comparisons among the above four standard simulations show that with increasing
436 aerosol concentrations in the main aerosol layer, there are decreases in solar radiation
437 reaching the surface due to the increasing interception of solar radiation by aerosols,
438 leading to decreases in cloud-liquid mass density, whether the main aerosol layer is in the
439 low atmosphere or in the upper atmosphere. Also, when there is the main aerosol layer in
440 the low atmosphere, there is radiative heating of air by aerosols around and below cloud
441 bases and this enables more instability, stronger updrafts and more cloud-liquid mass
442 despite less solar radiation reaching the surface than when there is the main aerosol layer
443 in the upper atmosphere, whether aerosol concentrations in the main layer is or low
444 (initially set at 1500 cm^{-3}) or high (initially set at 15000 cm^{-3})

445 The increase in cloud-liquid mass from the aro-above-cld-1500 run to the control-1500
446 run is smaller than that from the aro-above-cld run to the control run. This means that with
447 increasing concentrations of aerosols, the effects of radiative heating of aerosols, which is
448 in the low atmosphere, on instability and cloud-liquid mass enhances. This enhancement
449 is closely linked to the jump in the CAPE and updrafts that appears when concentration of
450 aerosols in the low atmosphere is high. Stated differently, the jump in the CAPE does not
451 occur when concentration of aerosols in the low atmosphere is low, meaning that there is
452 a critical value of initial aerosol concentrations above which the jump occurs.

453



454 **3.3 Comparisons between simulations with predicted and prescribed aerosol**
455 **concentrations**

456

457 Figure 7 shows the vertical distributions of aerosol concentrations, which are averaged over
458 the horizontal domain and simulation period, for the standard and repeated runs with no
459 temporal variation of aerosols (e.g., the control-novary, aro-above-cld-novary, control-
460 1500-novary, and aro-above-cld-1500-novary runs). Comparisons between the control and
461 control-novary runs (between the control-1500 and control-1500-novary runs) show that
462 due to the upward transportation of aerosols by updrafts in the control (control-1500) run,
463 aerosol concentrations in the main aerosol layer in the low atmosphere reduces and those
464 in the air above the main aerosol layer increases. This is as compared to the situation in the
465 control-novary (control-1500-novary) run where aerosols are assumed not to be affected
466 by cloud-induced wind (Figures 7a and 7c). Note that the low atmosphere is where cloud-
467 induced updrafts develop and grow, hence, the upward transportation of aerosols by them
468 is dominant. Due to the higher concentration of aerosols in the low atmosphere between
469 0.0 and ~1.0 km, there is more radiative heating of air by aerosols in the control-novary
470 run than in the control run and in the control-1500-novary run than in the control-1500 run
471 in the low atmosphere.

472 Comparisons between the aro-above-cld and aro-above-cld-novary runs (between the
473 aro-above-cld-1500 and aro-above-cld-1500-novary runs) show that due to the
474 transportation of aerosols by downdrafts in the aro-above-cld (aro-above-cld-1500) run,
475 aerosol concentrations in the main aerosol layer in the upper atmosphere reduces and those
476 in the air below the main aerosol layer increases. This is as compared to the situation in the
477 aro-above-cld-noary (aro-above-cld-1500-novary) run where aerosols are assumed not to
478 be affected by cloud-induced wind (Figures 7b and 7d). Note that the upper atmosphere is
479 where cloud-induced updrafts decelerate and turn into downdrafts, and the downward
480 transportation of aerosols by them is dominant. However, those increases in aerosol
481 concentrations in the air below the main aerosol layer mainly occur for the atmosphere
482 between ~1.5 and ~2.5 km and aerosol concentrations in the low atmosphere between 0.0
483 and ~1.0 km do not change significantly (Figures 7b and 7d). Hence, these transported
484 aerosols by downdrafts do not affect instability in the low atmosphere, which tends to have



485 more impacts on CAPE than instability in other parts of the atmosphere, significantly. This
486 leads to similar instability in the low atmosphere and CAPE, which in turn leads to similar
487 updrafts and cloud mass between the aro-above-cld and aro-above-cld-novary runs and the
488 aro-above-cld-1500 and aro-above-cld-1500-novary runs (Figure 8a). However, due to
489 more aerosols and their more radiative heating of air in the low atmosphere in the control-
490 novary run than in the control run and in the control-1500-novary run than in the control-
491 1500 run, there are higher CAPE (or greater instability), stronger updrafts and higher cloud
492 mass in the control-novary run than in the control run and in the control-1500-novary run
493 than in the control-1500 run (Figure 8a). It is notable that cloud mass in the control-novary
494 run is so large that its maximum value in the vertical profile as shown in Figure 8a exceeds
495 that even in the control-1500-novary run (Figure 8a). Associated with this, there are only
496 ~20 % changes in cloud mass between the control-1500 and control-1500-novary runs,
497 while there are as much as ~200 % changes in cloud mass between the control and control-
498 novary runs. This indicates that as aerosol concentration increases in the low atmosphere,
499 the sensitivity of responses of cloud mass to changes in aerosol concentrations, which are
500 induced by cloud-induced wind, in the low atmosphere increases substantially.

501

502 **3.4 Comparisons between simulations with aerosol radiative effects and those with** 503 **no aerosol radiative effects**

504

505 Figure 8b shows that with no aerosol radiative effects, differences in cloud mass between
506 the control-norad and aro-above-cld-norad runs are much smaller than those differences
507 between the control and aro-above-cld runs with aerosol radiative effects. However, as in
508 the control and aro-above-cld runs, there is higher cloud mass in the control-norad run,
509 which has the main aerosol layer in the low atmosphere, than in the aro-above-cld-norad
510 run, which has the main aerosol layer in the upper atmosphere. Figure 8b shows that cloud
511 mass in each of the control and aro-above-cld runs increases significantly when aerosol
512 radiative effects are turned off. Figure 8b shows that with no aerosol radiative effects,
513 differences in cloud mass between the control-1500-norad and aro-above-cld-1500-norad
514 runs are also smaller than those differences between the control-1500 and aro-above-cld-
515 1500 runs with aerosol radiative effects. However, as in the control-1500 and aro-above-



516 cld-1500 runs, there is higher cloud mass in the control-1500-norad run, which has the
517 main aerosol layer in the low atmosphere, than in the aro-above-cld-norad run, which has
518 the main aerosol layer in the upper atmosphere (Figure 8b). Figure 8b shows that cloud
519 mass in each of the control-1500 and aro-above-cld-1500 runs increases when aerosol
520 radiative effects are turned off, although these increases are a lot smaller than those in each
521 of the control and aro-above-cld runs. Here, we see that aerosol radiative effects suppress
522 clouds and reduce cloud mass. This means that effects of aerosol-induced reduction in the
523 surface-reaching solar radiation and subsequently in the surface heat fluxes on clouds are
524 dominant over those of radiative heating of air by aerosols, when it comes to the
525 explanation of differences in cloud mass between a situation with aerosol radiative effects
526 and that with no aerosol radiative effects. The suppression of clouds and reduction in cloud
527 mass increase with increasing aerosol concentrations in the main aerosol layer, whether the
528 main layer is in the low atmosphere or in the upper atmosphere, since more aerosols reduce
529 the surface-reaching solar radiation and surface heat fluxes more.

530 More aerosols and their activation (or nucleation of droplets) produce higher cloud
531 droplet number concentration (CDNC) in the low atmosphere in the control-1500-norad
532 run than in the aro-above-cld-1500-norad run. Note that aerosol activation mainly occurs
533 around cloud bases which are located in the low atmosphere. Droplets act as a source of
534 condensation, since individual droplets provide their surface areas onto which water vapor
535 condenses. Hence, higher CDNC induces more condensation and this in turn induces
536 stronger updrafts and more cloud mass in the control-1500-norad run than in the aro-above-
537 cld-1500-norad run. These effects of more aerosols, which induces more condensation and
538 stronger updrafts, are generally referred to as aerosol microphysical effects (Lee et al.,
539 2016). The differences in CDNC are greater due to greater differences in aerosols in the
540 low atmosphere between the control-norad and aro-above-cld-norad runs than those
541 between the control-1500-norad and aro-above-cld-1500-norad runs. This leads to greater
542 aerosol microphysical effects or greater differences in condensation, associated updrafts
543 and cloud mass between the control-norad and aro-above-cld-norad runs than those
544 between the control-1500-norad and aro-above-cld-1500-norad runs. With aerosol
545 radiative effects, radiative heating of air in the low atmosphere works in tandem with
546 aerosol microphysical effects. Hence, it is shown that as compared to the situation with no



547 aerosol radiative effects, with aerosol radiative effects, differences in cloud mass between
548 the run with the main aerosol layer in the low atmosphere and that with the layer in the
549 upper atmosphere are greater, whether aerosol concentrations are low (initially set at 1500
550 cm^{-3}) or high (initial set at 15000 cm^{-3}) in the layer. In addition to the jump in CAPE,
551 updrafts and condensation in the control run as described in Section 3.1, greater aerosol
552 microphysical effects in the low atmosphere when aerosol concentrations are high (initial
553 set at 15000 cm^{-3}) in the aerosol layer contributes to greater differences in cloud mass
554 between the control and aro-above-cld runs than between the control-1500 and aro-above-
555 cld-1500 runs when aerosol concentrations are low (initial set at 1500 cm^{-3}) in the aerosol
556 layer.

557 The initial concentration of aerosols in the aro-above-cld-norad run is identical to that
558 in the aro-above-cld-1500-norad run in the low atmosphere where most of aerosol
559 activation occurs as seen in the description of initial aerosol distribution in Section 2.2.
560 Due to this, in the low atmosphere, CDNC and condensation in the aro-above-cld-norad
561 run are similar to those in the aro-above-cld-1500-norad run. This leads to similar cloud
562 mass between the runs.

563

564 **4. Summary and conclusions**

565

566 This study examined differential impacts of an aerosol layer on warm cumulus clouds in
567 the Korean Peninsula between a situation where the main aerosol layer is located around
568 or above the tops of clouds in the upper atmosphere and that where the main aerosol layer
569 is located around or below the bottoms of clouds in the low atmosphere. This study finds
570 that the main layer intercepts more solar radiation which reaches the surface when it is in
571 the low atmosphere than when it is in the upper atmosphere. This makes the surface heat
572 fluxes and associated CAPE lower, which tend to make updrafts weaker and make cloud
573 mass lower when the main aerosol layer is in the low atmosphere. However, with the main
574 aerosol layer in the low atmosphere, there is a greater amount of cloud mass than that with
575 the main layer in the upper atmosphere. This is because the main layer in the low
576 atmosphere heats up the air there more, leading to increases in the instability and CAPE as
577 compared to the situation when the main layer is in the upper atmosphere. These increases



578 in CAPE are larger than reduction in CAPE due to the reduced solar radiation reaching the
579 surface, resulting in more cloud mass when the main layer is in the low atmosphere than
580 when the main layer is in the upper atmosphere.

581 With decreasing concentrations of aerosols in the main aerosol layer, there are
582 decreases in the interception of solar radiation reaching the surface, increases in surface
583 heat fluxes, CAPE and cloud mass whether the main layer is in the low atmosphere or in
584 the upper atmosphere. However, the decreasing concentrations of aerosols cause the jump
585 in instability as seen in the evolution of CAPE to disappear when the main layer is in the
586 low atmosphere. This leads to reducing differences in cloud mass between the situation
587 with the main layer in the low atmosphere and that with the layer in the upper atmosphere.
588 When the main aerosol layer is in the low atmosphere, with increasing aerosol
589 concentrations in the layer, the lifetime of cloud system reduces in a way that the lifetime
590 with the main layer in the low atmosphere gets shorter than that with the layer in the upper
591 atmosphere.

592 Updrafts and downdrafts in clouds transport aerosols. In particular, for the main aerosol
593 layer in the low atmosphere, updrafts transport aerosols in the main layer to places above
594 it. This reduces aerosol concentrations in the main layer, leading to reduction in radiative
595 heating of air by aerosols, CAPE, updrafts and cloud mass. This reduction enhances with
596 increasing aerosol concentrations in the main layer. For the aerosol layer in the upper
597 atmosphere, downdrafts transport aerosols in the layer to places below it. However, this
598 does not affect aerosol concentrations, radiative heating of air in the low atmosphere
599 significantly. This in turn does not affect CAPE and cloud mass significantly.

600 Aerosol radiative effects suppress clouds and reduce cloud mass by reducing solar
601 radiation which reaches the surface as compared to a situation when there are no aerosol
602 radiative effects. This suppression of clouds increases with increasing aerosol
603 concentrations in the main aerosol layer. Aerosol microphysical effects enhance cloud
604 mass and these effects are stronger with higher aerosol concentrations in the main layer.
605 When aerosol radiative effects, which are in terms of radiative heating of air by aerosols,
606 and aerosol microphysical effects work together, differences in cloud mass between a
607 situation where the main layer is in the upper atmosphere and that where the main layer is
608 in the low atmosphere enhance as compared to a situation where only aerosol



609 microphysical effects are present. More aerosols, and thus stronger radiative heating of air
610 and stronger aerosol microphysical effects in the main aerosol layer in the low atmosphere
611 enable this enhancement to be larger when aerosol concentrations are high in the main layer
612 than they are low.

613 This study shows that radiative heating of air by aerosols in the low atmosphere, which
614 are around or below cloud bases, enhances instability, invigorates convection and increases
615 cloud mass, which is contrary to the conventional wisdom of impacts of absorbing aerosols
616 on convection. However, radiative heating of air by aerosols in the upper atmosphere,
617 which are around or above cloud tops, enhances stability, suppresses convection and
618 reduces cloud mass. Aerosols in the low atmosphere intercept more solar radiation reaching
619 the surface, which tend to suppress the surface fluxes and convection, than aerosols in the
620 upper atmosphere. Here, we see that aerosol-induced changes in the surface fluxes and
621 those in radiative heating of air interact with each other in terms of responses of convection
622 and clouds to aerosols. This interaction varies with the varying vertical location of aerosols
623 and the varying cloud-induced wind that is at cloud scale. In general, traditional
624 parameterizations for warm cumulus clouds in climate and weather-forecast models have
625 not been able to consider this dependence of the interaction on the vertical location of
626 aerosols, since in general, those parameterizations for warm clouds do not differentiate
627 aerosol layers based on their vertical locations. In addition, the cloud-scale cloud-induced
628 wind, which is not able to be resolved by general resolutions in climate and weather-
629 forecast models, have not been represented by those parameterizations with good
630 confidence. So, impacts of aerosol transportation by cloud-induced wind on the interaction
631 have not been properly considered in those traditional parameterizations. Results here
632 demonstrate that for more comprehensive representation of interactions between warm
633 cumulus clouds and aerosols, we need to develop a more comprehensive parameterization
634 that is able well represent the varying interaction between aerosol-induced changes in the
635 surface fluxes and those in radiative heating of air with varying vertical locations of
636 aerosols and aerosol transportation by cloud-induced wind.

637

638

639



640 **Code/Data source and availability**

641

642 Our private computer system stores the code/data which are private and used in this study.

643 Upon approval from funding sources, the data will be opened to the public. Projects related

644 to this paper have not been finished, thus, the sources prevent the data from being open to

645 the public currently. However, if information on the data is needed, contact the

646 corresponding author Seoung Soo Lee (slee1247@umd.edu).

647

648 **Author contributions**

649 Essential initiative ideas are provided by SSL, JU and WJC to start this work. Simulation

650 and observation data are analyzed by SSL, JU and KJH. CHJ. JG and YZ review the results

651 and contribute to their improvement.

652

653 **Competing interests**

654 The authors declare that they have no conflict of interest.

655

656

657

658

659

660

661

662

663

664

665

666

667

668

669

670

671

672

673

674

675

676

677

678

679



680 **Acknowledgements**

681

682 This study is supported by the National Research Foundation of Korea (NRF) grant funded
683 by the Korea government (MSIT) (No. NRF2020R1A2C1003215 and No.
684 2020R1A2C1013278) and the “Construction of Ocean Research Stations and their
685 Application Studies” project, funded by the Ministry of Oceans and Fisheries, South Korea.

686 This study is also supported by Basic Science Research Program through the NRF funded
687 by the Ministry of Education (No. 2020R1A6A1A03044834).

688

689

690

691

692

693

694

695

696

697

698

699

700

701

702

703

704

705

706

707

708

709

710



711 **References**

712

713 Albrecht, B. A.: Aerosols, cloud microphysics, and fractional cloudiness, *Science*, 245,
714 1227-1230, 1989.

715 Brown, A., Milton, S., Cullen, M., Golding, B., Mitchell, J., and Shelly, A.: Unified
716 modeling and prediction of weather and climate: A 25-year journey, *Bull. Am*
717 *Meteorol. Soc.* 93, 1865–1877, 2012.

718 Chen, F., and Dudhia, J.: Coupling an advanced land-surface hydrology model with the
719 Penn State-NCAR MM5 modeling system. Part I: Model description and
720 implementation, *Mon. Wea. Rev.*, 129, 569–585, 2001.

721 de Graaf, M., Bellouin, N., Tilstra, L.G., Haywood, J., Stammes, P.: Aerosol direct radiative
722 effect of smoke over clouds over the southeast Atlantic Ocean from 2006 to 2009.
723 *Geophys. Res. Lett.* 41, 7723-7730, 2014.

724 Fan, J., Yuan, T., Comstock, J. M., et al.: Dominant role by vertical wind shear in regulating
725 aerosol effects on deep convective clouds, *J. Geophys. Res.*, 114,
726 doi:10.1029/2009JD012352, 2009.

727 Feingold, G., H. Jiang, H., and J. Y. Harrington, J. Y.: On smoke suppression of clouds in
728 Amazonia, *Geophys. Res. Lett.*, 32, L02804, doi:10.1029/2004GL021369, 2005.

729 Forster, P., et al., Changes in atmospheric constituents and in radiative forcing, in: *Climate*
730 *change 2007: the physical science basis, Contribution of working group I to the Fourth*
731 *Assessment Report of the Intergovernmental Panel on Climate Change*, edited by
732 Solomon, S., et al., Cambridge Univ. Press, New York, 2007.

733 Formenti, P., B. D’Anna, C. Flamant, et al.: The Aerosols, Radiation and Clouds in
734 Southern Africa Field Campaign in Namibia: Overview, illustrative observations, and
735 way forward, *Bull. Amer. Meteor. Soc.*, 100, 1277-1298, 2019.

736 Hahn, C. J., and Warren, S. G.: A gridded climatology of clouds over land (1971–96) and
737 ocean (1954–97) from surface observations worldwide. *Numeric Data Package NDP-*
738 *026EORNL/CDIAC-153*, CDIAC, Department of Energy, Oak Ridge, TN, 2007.

739 Hansen, J. E., Sato, M. and Ruedy, R.: Radiative forcing and climate response, *J. Geophys.*
740 *Res.*, 102, 6831–6864, 1997.

741 Hartmann, D. L., Ockert-Bell, M. E., and Michelsen, M. L.: The effect of cloud type on



- 742 earth's energy balance—Global analysis, *J. Climate*, 5, 1281–1304, 1992.
- 743 Haywood, J. M. and Shine, K. P.: Multi-spectral calculations of the radiative forcing of
744 tropospheric sulfate and soot aerosols using a column model, *Q. J. R. Meteorol. Soc.*,
745 123, 1907–1930, 1997.
- 746 Holben, B. N., Tanré, D., Smirnov, et al.: An emerging ground-based aerosol climatology:
747 Aerosol optical depth from AERONET, *J. Geophys. Res.*, 106, 12067–12097, 2001.
- 748 Johnson, B. T., Shine, K. P., and Forster, P. M.: The semi-direct aerosol effect: Impact of
749 absorbing aerosols on marine stratocumulus, *Q. J. R. Meteorol. Soc.*, 130, 1407– 1422,
750 2004.
- 751 Khain, A., Pokrovsky, A., Rosenfeld, D., Blahak, U., and Ryzhkoy, A.: The role of CCN in
752 precipitation and hail in a mid-latitude storm as seen in simulations using a spectral
753 (bin) microphysics model in a 2D dynamic frame, *Atmos. Res.*, 99, 129–146, 2011.
- 754 Lee, S. S., Guo, J. M., and Li, Z.: Delaying precipitation by air pollution over the Pearl
755 River Delta. Part II: Model simulations, *J. Geophys. Res.*, 121, 11739–11760.
- 756 Lee, S. S., Ha, K.-J., Manoj, M. G., et al.: Midlatitude mixed-phase stratocumulus
757 clouds and their interactions with aerosols: how ice processes affect microphysical,
758 dynamic, and thermodynamic development in those clouds and interactions?, *Atmos.*
759 *Phys. Chem.*, 21, 16843–16868, 2021.
- 760 McFarquhar, G. M. and Wang, H.: Effects of Aerosols on Trade Wind Cumuli over the
761 Indian Ocean: Model Simulations, *Q. J. R. Meteorol. Soc.*, 132, 821–843, 2006.
- 762 Mlawer, E. J., Taubman, S. J., Brown, P. D., Iacono, M. J., and Clough, S. A.: RRTM, a
763 validated correlated-k model for the longwave, *J. Geophys. Res.*, 102, 16663–16668,
764 1997.
- 765 Ramaswamy, V., et al.: Radiative forcing of climate change, in *Climate Change 2001: The*
766 *Scientific Basis*, edited by J. T. Houghton et al., 349–416, Cambridge Univ. Press,
767 New York, 2001.
- 768 Redemann, J., Wood, R., Zuidema, P., et al.: An overview of the ORACLES (ObseRvations
769 of Aerosols above CLouds and their intERactionS) project: aerosol–cloud–radiation
770 interactions in the southeast Atlantic basin, *Atmos. Chem. Phys.*, 21, 1507–1563, 2021.
- 771 Stephens, G. L., and Greenwald, T. J.: Observations of the Earth's radiation budget in
772 relation to atmospheric hydrology. Part II: Cloud effects and cloud feedback. *J.*



- 773 Geophys. Res., 96, 15 325–15 340, 1991.
- 774 Tao, W.-K., Chen, J.-P., Li, Z., Wang, C., and Zhang C., Impact of aerosols on convective
775 clouds and precipitation, *Rev. Geophys.*, 50, RG2001, doi:10.1029/2011RG000369,
776 2012.
- 777 Twomey, S.: The influence of pollution on the shortwave albedo of clouds, *J. Atmos. Sci.*,
778 34, 1149-1152, 1977.
- 779 Twomey, S.: Pollution and the Planetary Albedo, *Atmos. Env.*, 8, 1251-1256, 1974.
- 780 Wang, H., Skamarock, W. C., and Feingold, G.: Evaluation of scalar advection schemes in
781 the Advanced Research WRF model using large-eddy simulations of aerosol-cloud
782 interactions, *Mon. Wea. Rev.*, 137, 2547-2558, 2009.
- 783 Warren, S. G., Hahn, C. J., London, J., Chervin, R. M., and Jenne, R. L.: Global distribution
784 of total cloud cover and cloud types over land. NCAR Tech. Note NCAR/TN-
785 273+STR, National Center for Atmospheric Research, Boulder, CO, 29 pp. + 200
786 maps, 1986.
- 787 Wood, R.: Stratocumulus clouds, *Mon. Wea. Rev.*, 140, 2373-2423, 2012.
- 788 Xu, H., Guo, J., Wang, Y., et al.: Warming effect of dust aerosols modulated by overlapping
789 clouds below, *Atmos. Env.*, 166, 2017, 393-402, 2017.
- 790
- 791
- 792
- 793
- 794
- 795
- 796
- 797
- 798
- 799
- 800
- 801
- 802
- 803
- 804
- 805
- 806
- 807
- 808
- 809



810 **FIGURE CAPTIONS**

811

812 Figure 1. An inner rectangle in the map of the Korean Peninsula represents the simulation
813 domain. The green (light blue) represents land (ocean) area in the map.

814

815 Figure 2. Vertical distributions of potential temperature and water-vapor mixing ratio at
816 09:00 LST on April 15th, 2015. These distributions are obtained from radiosonde sounding
817 near the simulation domain in Figure 1.

818

819 Figure 3. Vertical distributions of the area-averaged aerosol concentrations at the first time
820 step of (a) the control run and (b) the aro-above-cld run.

821

822 Figure 4. Vertical distributions of the time- and area-averaged cloud-liquid mass density
823 that represents cloud mass for the standard simulations (i.e., the control, aro-above-cld,
824 control-1500 and aro-above-cld-1500 runs).

825

826 Figure 5. Time series of the domain-averaged (a) liquid-water path, (b) updraft speed, (c)
827 condensation rate and (d) convective available potential energy in the standard simulations.

828

829 Figure 6. Vertical distributions of the time- and area-averaged radiative heating rate (a) in
830 the control and aro-above-cld runs over the initial stage between 10:00 and 13:50 LST, (b)
831 in the control and aro-above-cld runs over the whole simulation period and (c) in the
832 control-1500 and aro-above-cld-1500 runs over the whole simulation period.

833

834 Figure 7. Vertical distributions of the time- and area-averaged aerosol concentrations (a)
835 in the control and control-novary runs, (b) aro-above-cld and aro-above-cld-novary runs,
836 (c) control-1500 and control-novary-1500 runs and (d) aro-above-cld-1500 and aro-above-
837 cld-novary-1500 runs.

838

839 Figure 8. Vertical distributions of the time- and area-averaged cloud-liquid mass density.
840 In (a), the control-novary, aro-above-cld-novary, control-1500-novary and aro-above-cld-



841 1500-novary runs and in (b), the control-norad, aro-above-cld-norad, control-1500-norad
842 and aro-above-cld-1500-norad runs are shown together with the standard simulations.

843

844

845

846

847

848

849

850

851

852

853

854

855

856

857

858

859

860

861

862

863

864

865

866

867

868

869

870

871



| Simulations | Altitudes of a main aerosol layer (km) | Aerosol concentrations in the main aerosol layer at the first time step (cm^{-3}) | Aerosol evolution | Aerosol radiative effects |
|---------------------------|--|--|-------------------|---------------------------|
| Control | 0 - 1 | 15000 | Present | Present |
| Aro-above-cld | 2.5-3.5 | 15000 | Present | Present |
| Control-1500 | 0 - 1 | 1500 | Present | Present |
| Aro-above-cld-1500 | 2.5-3.5 | 1500 | Present | Present |
| Control-novary | 0 - 1 | 15000 | Absent | Present |
| Aro-above-cld-novary | 2.5-3.5 | 15000 | Absent | Present |
| Control-1500-novary | 0 - 1 | 1500 | Absent | Present |
| Aro-above-cld-1500-novary | 2.5-3.5 | 1500 | Absent | Present |
| Control-norad | 0 - 1 | 15000 | Present | Absent |
| Aro-above-cld-norad | 2.5-3.5 | 15000 | Present | Absent |
| Control-1500-norad | 0 - 1 | 1500 | Present | Absent |
| Aro-above-cld-1500-norad | 2.5-3.5 | 1500 | Present | Absent |

872

873 Table 1. Summary of simulations

874

875

876

877

878

879

880

881

882

883

884

885



| Simulations | Net solar radiation flux reaching the surface (W m^{-2}) | Surface latent heat fluxes (W m^{-2}) | Surface sensible heat fluxes (W m^{-2}) | Surface latent heat fluxes plus surface sensible heat fluxes (W m^{-2}) |
|--------------------|---|--|--|--|
| Control | 293 (205) | 175 (120) | 22 (16) | 197 (136) |
| Aro-above-cld | 306 (217) | 170 (117) | 48 (33) | 218 (150) |
| Control-1500 | 461 | 250 | 70 | 320 |
| Aro-above-cld-1500 | 467 | 248 | 75 | 323 |

886

887 Table 2. The time- and area-averaged net solar radiation, latent heat, sensible heat and total
888 heat (sensible plus latent heat) fluxes at the surface over the whole simulation period in the
889 standard simulations. Numbers in the parentheses are averaged over the initial period
890 between 10:00 and 13:50 LST for control and aro-above-cld runs.

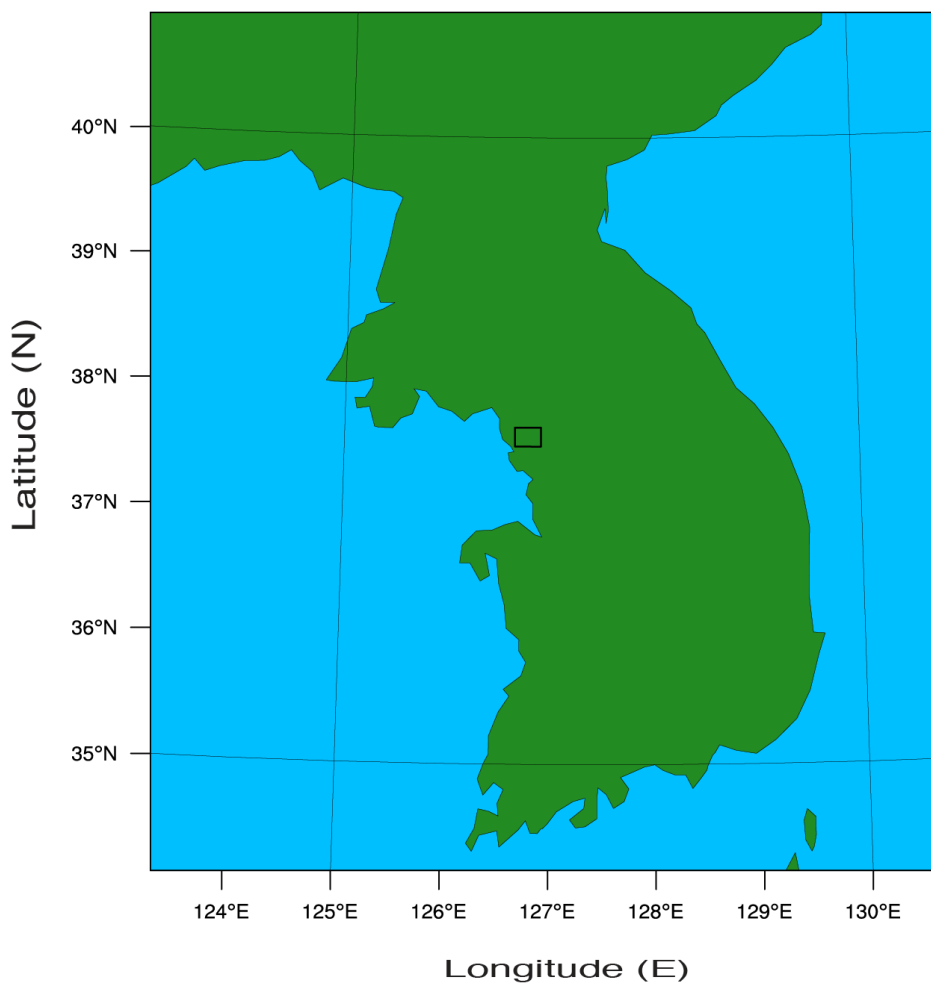


Figure 1

891

892

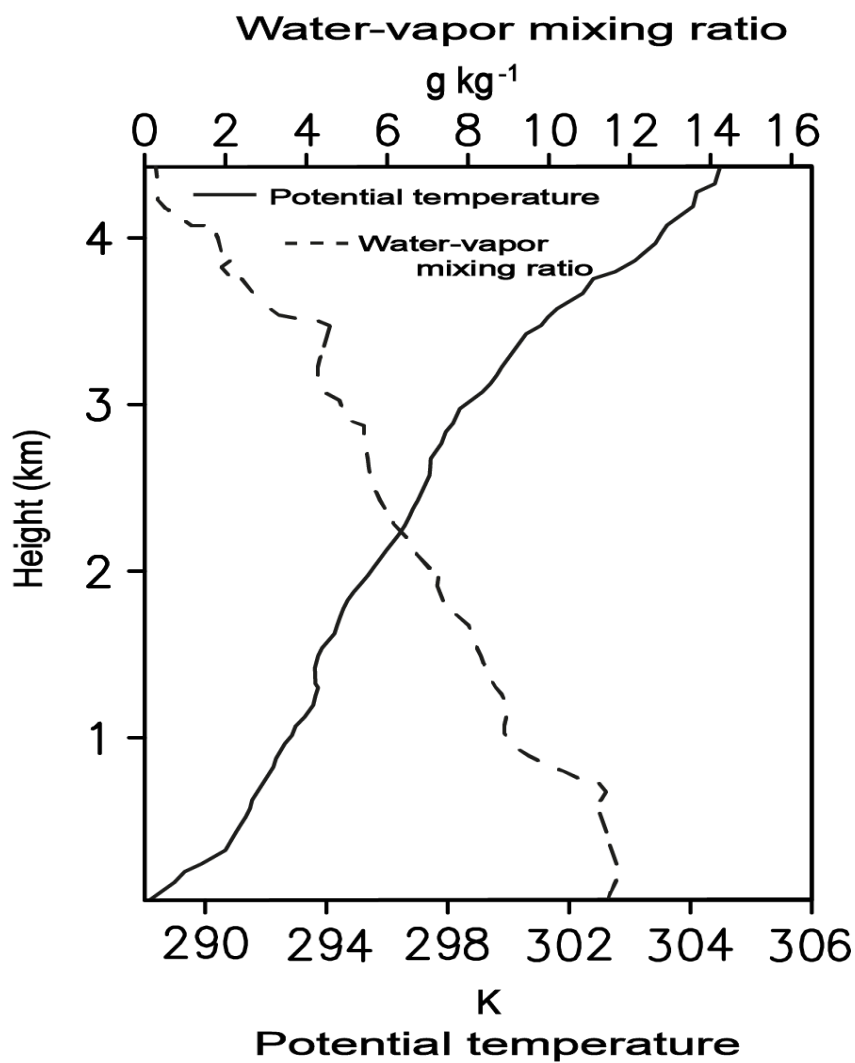
893

894

895

896

897



898

899

900

901

902

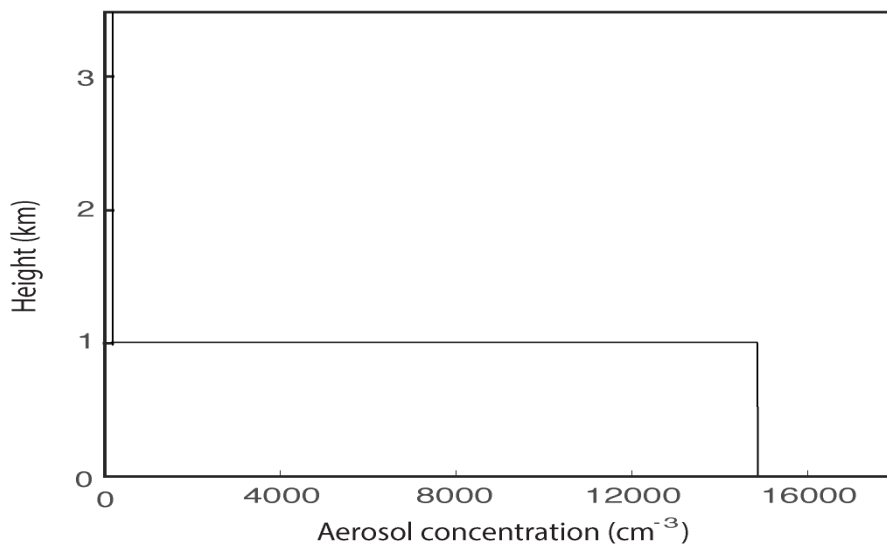
903

Figure 2

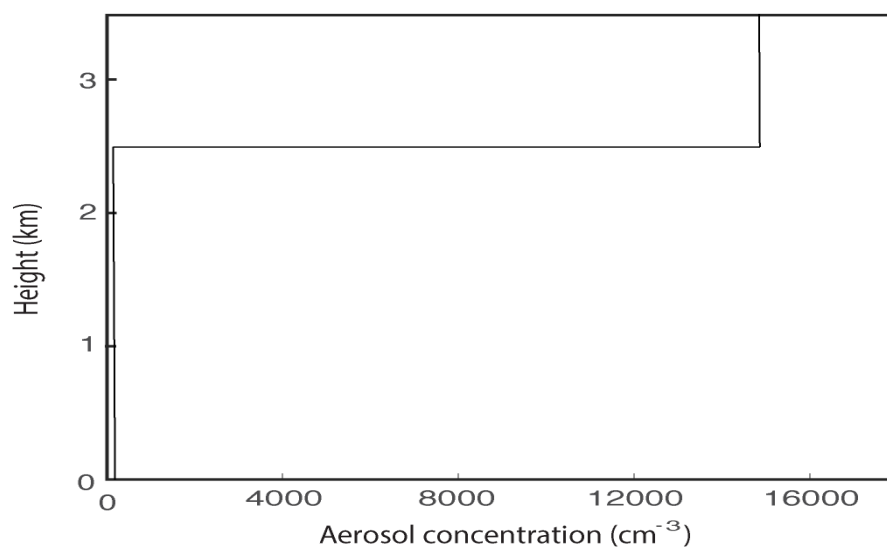


Vertical distributions of aerosol concentrations

a



b

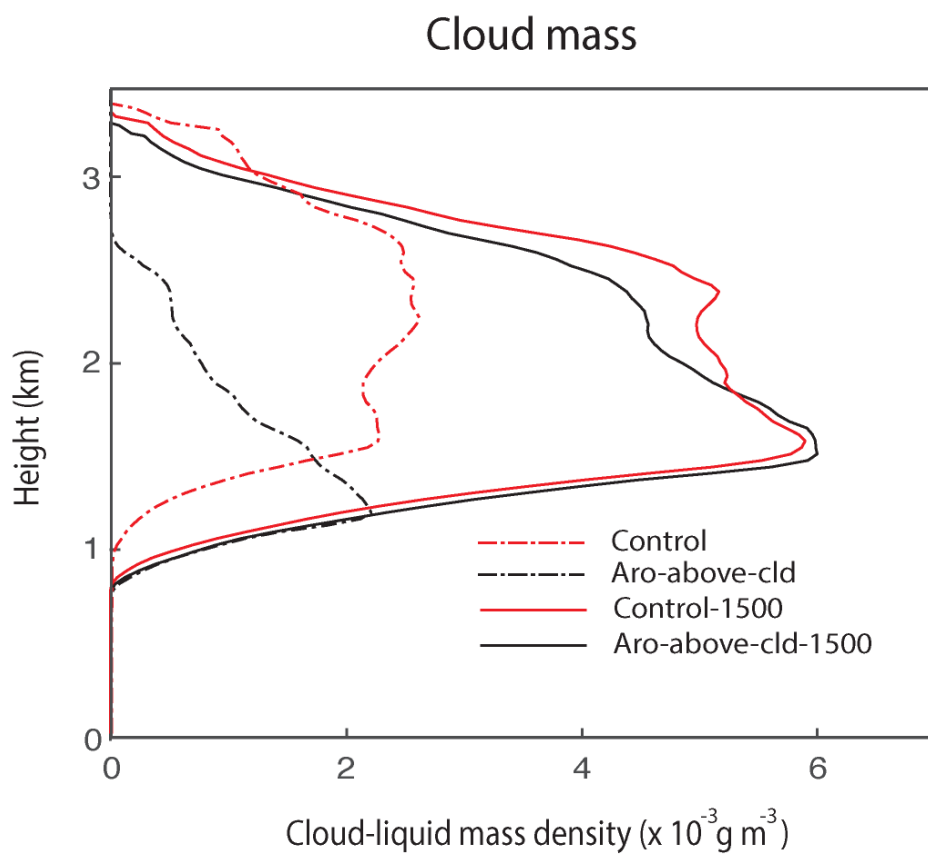


904

905

906

Figure 3



907

908

Figure 4

909

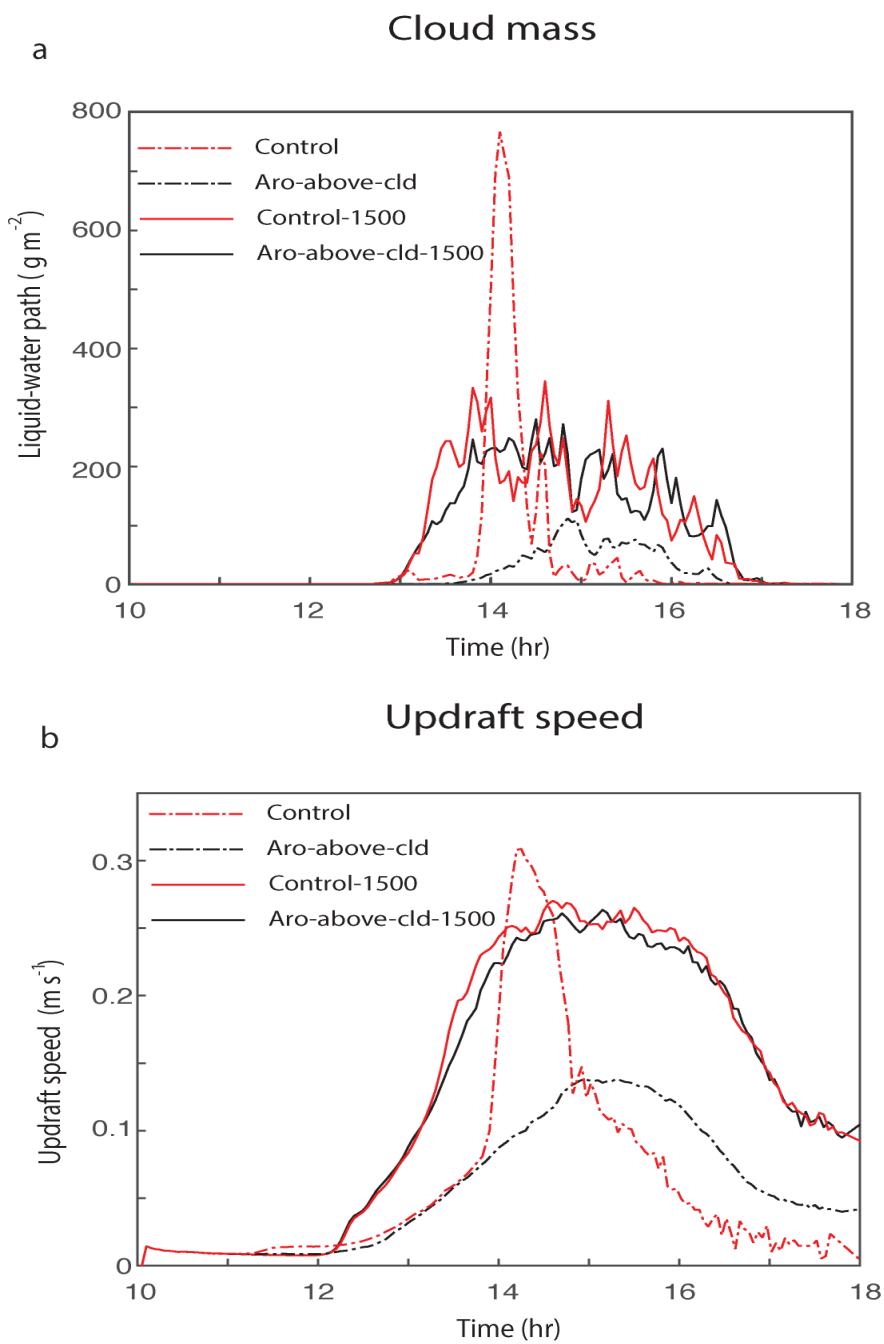
910

911

912

913

914

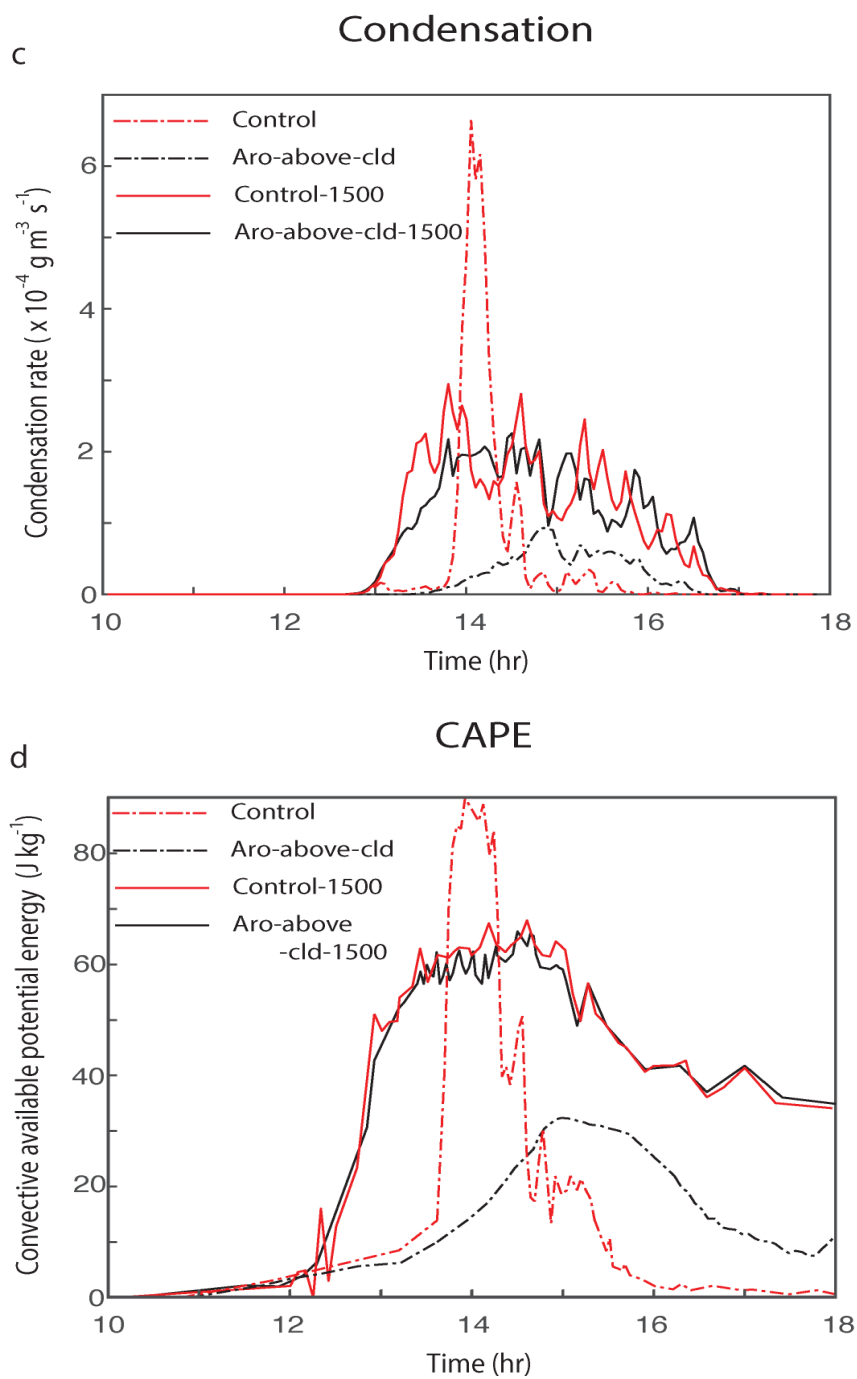


915

916

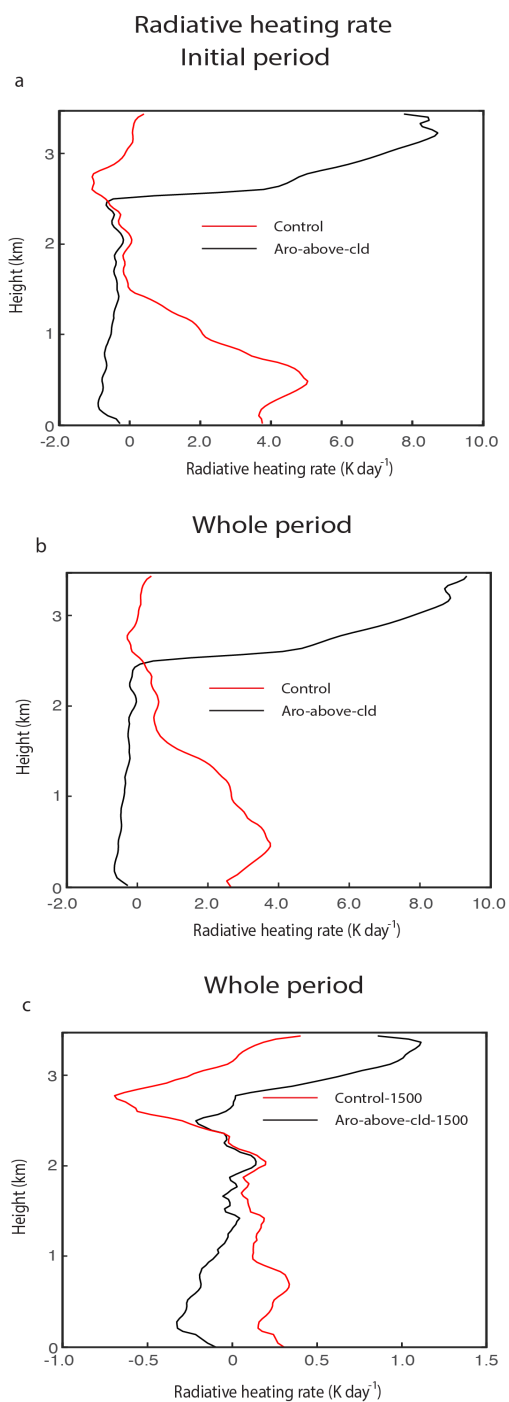
917

Figure 5



918
919

Figure 5

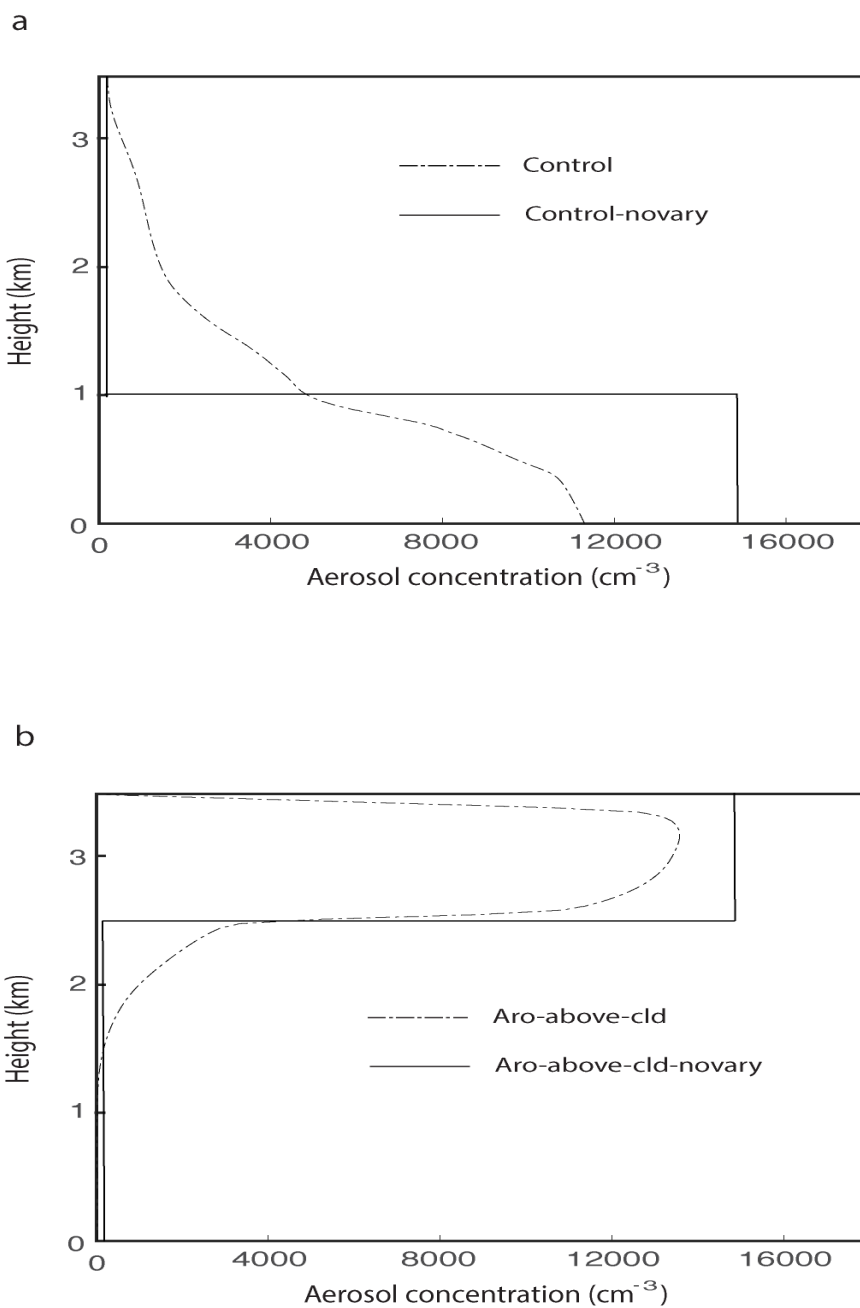


920
921
922

Figure 6

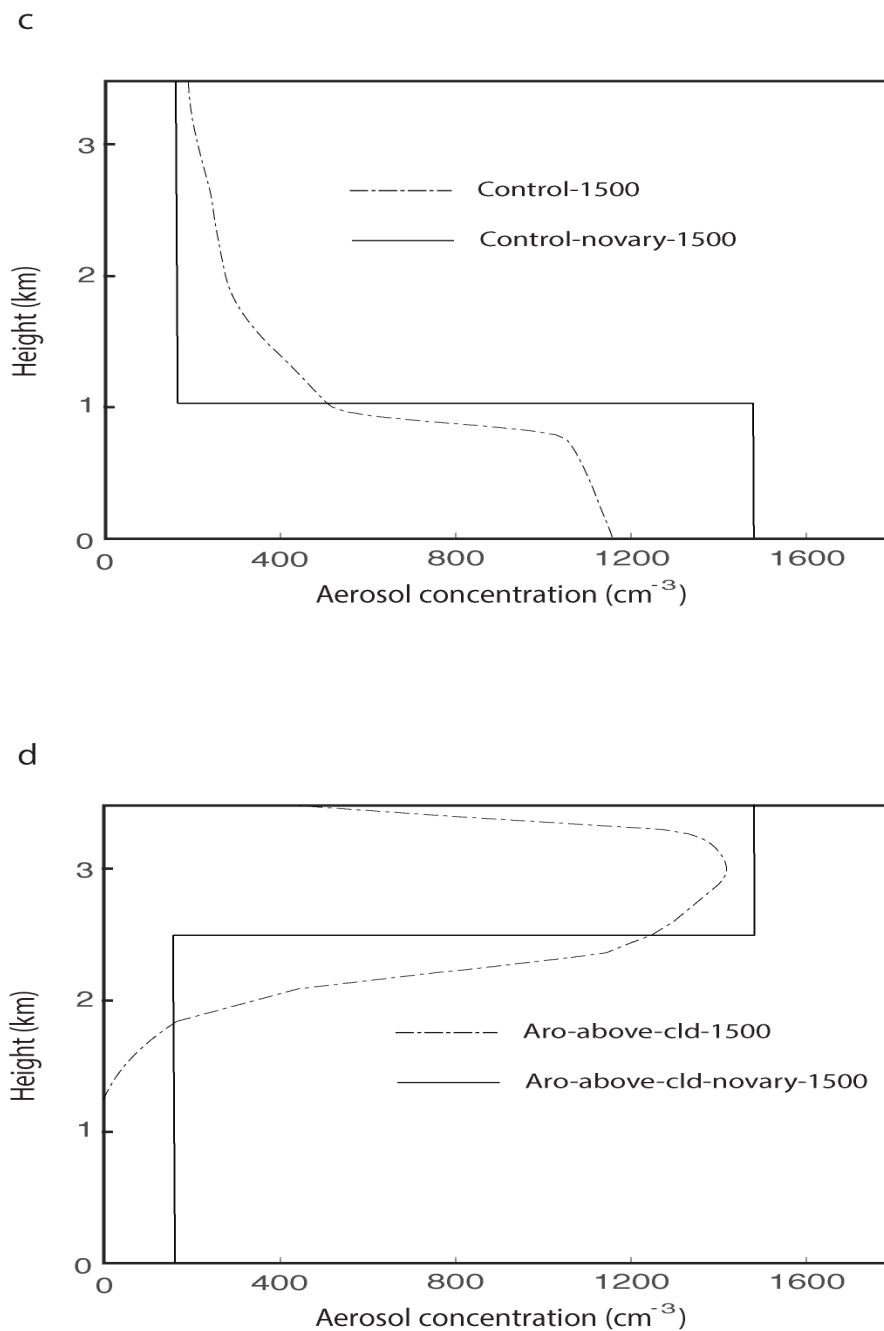


Vertical distributions of aerosol concentrations



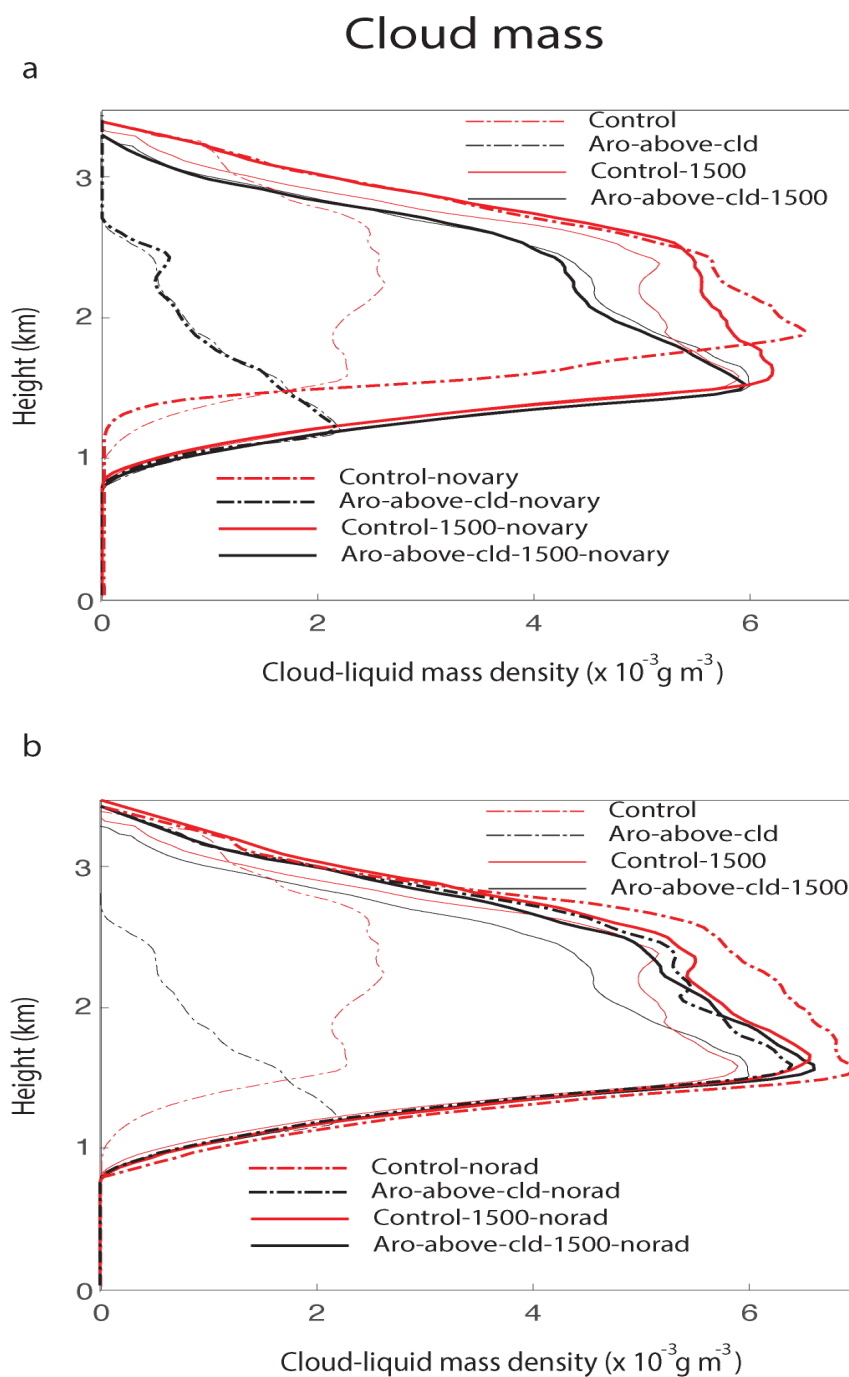
923
924
925

Figure 7



926
927
928
929

Figure 7



930
931
932

Figure 8